NOSA, an analytical toolbox for multicellular optical electrophysiology

Sebastian Oltmanns[1], Frauke Sophie Abben[1], Anatoli Ender[2], Sophie Aimon[3], Richard Kovacs[1], Stephan J Sigrist [2, 4, 5], Douglas A Storace[6], Jörg R P Geiger[1] and Davide Raccuglia[1]

1 Institute of Neurophysiology, Charité – Universitätsmedizin Berlin, corporate member of Freie Universität Berlin and Humboldt-Universität zu Berlin, and Berlin Institute of Health, Charitéplatz 1, 10117 Berlin, Germany

2 German Center for Neurodegenerative Disorders, Charité – Universitätsmedizin Berlin, Charitéplatz 1, 10117 Berlin, Germany

3 School of Life Sciences, Technical University Munich, 85354 Freising, Germany

4 Institute for Biology/Genetics, Freie Universität Berlin, Takustrasse 6, 14195 Berlin, Germany

5 NeuroCure, Charité – Universitätsmedizin Berlin, corporate member of Freie Universität Berlin and Humboldt-Universität zu Berlin, and Berlin Institute of Health, Charitéplatz 1, 10117 Berlin, Germany

6 Florida State University, Department of Biological Science, Tallahassee, FL 32306

lead contact: davide.raccuglia@charite.de

Abstract

Understanding how neural networks generate activity patterns and communicate with each other requires monitoring the electrical activity from many neurons simultaneously. Perfectly suited tools for addressing this challenge are genetically encoded voltage indicators (GEVIs) because they can be targeted to specific cell types and optically report the electrical activity of individual, or populations of neurons. However, analyzing and interpreting the data from voltage imaging experiments is challenging because high recording speeds and properties of current GEVIs yield only low signal-to-noise ratios, making it necessary to apply specific analytical tools. Here, we present NOSA (Neuro-Optical Signal Analysis), a novel open source software designed for analyzing voltage imaging data and identifying temporal interactions between electrical activity patterns of different origin.

In this manuscript we explain the challenges that arise during voltage imaging experiments and provide hands-on analytical solutions. We demonstrate how NOSA's baseline fitting, filtering algorithms and movement correction can compensate for shifts in baseline fluorescence and extract electrical patterns from low signal-to-noise recordings. Moreover, NOSA contains powerful features to identify oscillatory frequencies in electrical patterns and extract neuronal firing characteristics. NOSA is the first open-access software to provide an option for analyzing simultaneously recorded optical and electrical data derived from patch-clamp or other electrode-based recordings. To identify temporal relations between electrical activity patterns we implemented different options to perform cross correlation analysis, demonstrating their utility during voltage imaging in *Drosophila* and mice. All features combined, NOSA will facilitate the first steps into using GEVIs and help to realize their full potential for revealing cell-type specific connectivity and functional interactions. If you would like to test NOSA, please send an email to the lead contact.

Introduction

One goal of The American BRAIN initiative was to develop methods to comprehend complex activity patterns in specific brain networks and even in whole brains (Alivisatos et al., 2012). One crucial step towards gaining insight into the mechanisms and interactions of neural activity patterns is the development of tools that allow for measuring multi-cellular electrical activity and analyzing their complex datasets (Alivisatos et al., 2012).

Genetically encoded voltage indicators (GEVIs) have emerged as promising tools for measuring neural electrical activity (Lin and Schnitzer, 2016; Yang and St-Pierre, 2016). GEVIs are powerful tools, in part because they can be genetically targeted to specific neural populations and optically report the electrical activity from many neurons simultaneously, and even from neuropil that is otherwise inaccessible to classical electrophysiology. GEVIs have been successfully used for monitoring multicellular activity and population dynamics in *Drosophila* (Cao et al., 2013; Raccuglia et al., 2016; Aimon et al., 2019; Raccuglia et al., 2019), visual and olfactory responses in mice (Gong et al., 2015; Storace et al., 2015; Storace and Cohen, 2017), cerebellar activity in Zebrafish (Miyazawa et al., 2018) and also pharyngeal activity in *C. elegans* (Azimi Hashemi et al., 2019).

Although GEVIs are being continually improved (Lin and Schnitzer, 2016; Storace et al., 2016), high recording speeds, low signal-to-noise ratios (SNR) and GEVI-specific kinetics bring about unique challenges with respect to data analysis (Yang and St-Pierre, 2016; Kulkarni and Miller, 2017) and thus require the development of adequate processing tools. Yet, there is currently no freely available software, which combines processing tools addressing these challenges with analytical tools for identifying specific activity patterns, temporal relations and functional interactions.

Here we present NOSA (Neuro-Optical Signal Analysis) – an open source software designed specifically for the analysis of multicellular optical electrophysiology. NOSA features baseline fitting and filtering algorithms to extract electrical patterns from high speed recordings with low SNR. Moreover, NOSA provides analytical tools for identifying specific activity patterns and their temporal relation via functions that provide spectral and cross-correlation analysis. NOSA also includes features for spike- and burst detection, movement artefact compensation, and the ability to analyze simultaneously performed optical and electrical recordings. With these analytical tools, intuitive design, and convenient graphical interface, NOSA should greatly facilitate the first steps into using GEVIs, enabling laboratories around the world to perform and analyze multicellular voltage imaging recordings.

Results

NOSA Interface and overview of processing tools

Our software package NOSA (**Fig. 1**) is designed to process and analyze voltage imaging recordings. Recordings can be imported into NOSA as tif/tiff files, which can be temporally cropped (the user can select a specific time window) or corrected for movement artefacts (**Fig. 1A**). NOSA automatically calculates the relative changes in fluorescence for selected regions of interest (ROIs) (**Fig. 1B, C**) after factoring in recording speed, background correction as well as selected fitting (e.g., exponential drift correction) and filtering algorithms (**Fig. 1D**). Activity patterns from different ROIs (e.g., cells) can be displayed in one plot to facilitate comparisons, although the user can easily switch to a more detailed view of the currently selected ROI (**Fig. 1E**).

Because most GEVIs exhibit decreases in their fluorescence in response to depolarization, NOSA provides the option to invert the relative changes (**Fig. 1B**). To generate ROI masks, selected ROIs can be copied and pasted into other recordings (**Fig. 1B**). All data extracted by NOSA can be exported as spreadsheet files (**Fig. 1B**).

As high recording speeds generate a larger number of frames, we included simple but efficient options to increase software performance. For example, the recording frequency can be reduced by applying different interpolation algorithms (**Fig. 1B,** right-click on file name). To simplify the simultaneous evaluation of multiple recordings this method can also be used to unify different recording speeds. However, this method should only be used when the recording frequency is higher than needed to resolve single depolarization events. Moreover, software performance can be increased by using a rectangular ROI instead of an elliptical and by deselecting the live preview mode. In the live preview mode, changes in relative fluorescence are displayed while moving around a ROI. After deselecting live preview mode (**Fig. 1C,** right-click), changes in relative fluorescence are only displayed after placing the ROI.

NOSA features power spectrum analysis as well as spike and burst detection to analyze activity patterns (**Fig. 1F, G**). The event shape feature uses detected events to display the average firing characteristics of a neuron. To analyze temporal relations and functional interactions between activity patterns, cross correlation can be performed on detected events and on the relative changes in fluorescence (**Fig. 1H**). Via the control panel all features can be controlled (**Fig. 1I**) for each ROI independently and settings selected for one ROI can easily be applied to all other ROIs.

114 **Multicellular optical electrophysiology**

115 To demonstrate the utility of NOSA we used *Drosophila* to express the genetically encoded
116 voltage indicator (GEVI) ArcLight in ellipsoid body R5 ring neurons and the GEVI Varnam in
117 fan-shaped neurons (**Fig. 2**). Both neural structures are considered to be integration centers
118 for various sensory modalities (Seelig and Jayaraman, 2013; Green et al., 2017; Sun et al.,
119 2017; Hu et al., 2018) and play important roles in locomotion (Strauss and Heisenberg, 1993)
120 and sleep regulation (Donlea et al., 2014; Liu et al., 2016; Donlea et al., 2018; Guo et al.,
121 2018; Raccuglia et al., 2019).

122 After setting a ROI, the optical trace should first be corrected for shifts in baseline
123 fluorescence (e.g. due to photoisomerization and bleaching). Several baseline correction
124 algorithms are included (**Suppl. Fig. 1-3**), and the user can set additional baseline markers
125 to guide the fitting curve for more complex shifts in baseline fluorescence (**Suppl. Fig. 1A**).
126 After baseline correction, smoothing and inversion of the raw fluorescence (depolarization
127 leads to a reduction in fluorescence), the electrical patterns of single R5 ring neurons
128 become apparent (**Fig. 2A, compare Suppl. Fig. 1**). A power spectrum analysis revealed
129 that single R5 neurons oscillate between 0.5 – 1.5 Hz (**Fig. 2B**). We recently reported that
130 R5 oscillations within this spectrum are linked to the fly's sleep quality because they facilitate
131 consolidated sleep phases (Raccuglia et al., 2019). The cross-correlation function built into
132 NOSA provides a simple way of visualizing the temporal relation between the electrical
133 patterns of the different cells (**Fig. 2C**). The cross correlogram indicates that electrical
134 patterns of cells 1, 2 and 3 largely overlap (main phase lag at 0) while cell 4 is out of phase
135 (**Fig. 2C**). We also implemented the option to perform a cross correlation on instantaneous
136 amplitudes (Adhikari et al., 2010) and use a band pass filter for comparing temporal relations
137 within a specific frequency range.

138 Due to the relatively low recording speed (78 Hz) and the slow kinetics of ArcLight we could
139 not resolve single spikes in this example (**Fig. 2A**). By increasing the recording speed to 160
140 Hz and taking advantage of the improved kinetics of the red-shifted GEVI Varnam (Kannan
141 et al., 2018), we resolved single action potentials within the electrical activity of dorsal fan-
142 shaped body neurons (**Fig. 2D, E**). Compared to ArcLight, the SNR is lower and thus the
143 detection of spikes heavily depends on the imaging conditions (**Fig. 2D**), as individual spikes
144 could not be resolved in the dimmer cells (**Fig. 2D, see cell3**).

145 That said, several functions are included to facilitate spike detection in low signal-to-noise
146 recordings. This includes several filtering algorithms (see next chapter) as well as the ability
147 to semi-automatically detect spikes and visualize their average shape using the event-shape
148 feature (**Fig. 2F, compare Suppl. Fig. 2**). Moreover, the temporal relation between detected

149 spikes can be analyzed using the spike cross correlation feature (**Fig. 2G, compare Suppl.**
150 **Fig. 2**).

151 **Spike and burst detection**

152 In NOSA, electrical characteristics of single neurons as well as the kinetics of different GEVIs
153 can be analyzed in detail using event detection features. To demonstrate this, we compare
154 the GEVIs ArcLight and Ace2N (Gong et al., 2015) in R5 neurons in *Drosophila*. While most
155 R5 neurons burst (~90%), some mainly spike (Liu et al., 2016). NOSA's spike detection and
156 event shape feature was used to analyze two spiking R5 neurons expressing either ArcLight
157 or Ace2N (**Fig. 3A-B**). While the kinetics of the depolarization are comparable, the
158 repolarization is considerably slower in ArcLight, which is in accordance with previous
159 findings indicating that Ace2N has faster kinetics (Gong et al., 2015).

160 Optical representations of action potentials do not only depend on the GEVI kinetics, but also
161 on a sensitive interplay between recording-speed and signal-to-noise ratio. To demonstrate
162 this, action potentials were imaged using Ace2N at either 250 Hz or 1000 Hz (**Fig. 3C**). The
163 faster recording speed resulted in a drastically reduced signal-to-noise ratio, making action
164 potentials barely detectable (**Fig. 3C**). However, filtering algorithms provided in NOSA can
165 increase the signal-to-noise ratio and thus the spike detection fidelity, as demonstrated here
166 by using the Savitzky-Golay algorithm (**Fig. 3C**). Automatic averaging of detected spikes
167 (event shape) indicates that the temporal features of single action potentials are well
168 represented at 250 Hz (**Fig. 3D**). Here, the limiting factors seem to be the temporal dynamics
169 of the GEVI itself.

170 An advantage of enhanced temporal dynamics of a GEVI becomes apparent when analyzing
171 high-frequency spikes in bursting neurons (**Fig. 3E**). Using Ace2N, spikes riding on top of
172 bursts are more likely to be resolved and are therefore more readily detectable (**Fig. 3F**).
173 However, the event shape feature indicates that the temporal characteristics of the bursts are
174 identical but ArcLight produces a bigger change in relative fluorescence (**Fig. 3G**). This is
175 likely due to the slower kinetics of ArcLight, resulting in several spikes probably merging into
176 one "spike".

177 **Movement and background correction**

178 Due to a relatively small SNR, movement artefacts are especially problematic for *in vivo*
179 voltage imaging. We therefore implemented several movement correction algorithms into
180 NOSA. We here demonstrate the symmetric diffeomorphic algorithm, which was originally
181 designed for detecting brain deformations during magnetic resonance imaging (Avants et al.,
182 2008). This sophisticated algorithm is very time consuming but shows impressive results
183 (**Fig. 4A**). Single R5 neurons recorded *in vivo* show substantial movement artefacts (**Fig.**

184 **4A**). However, after performing the symmetric diffeomorphic algorithm electrical activity can
185 be recovered even during periods of heavy movement.

186 Scattering light can also reduce the signal-to-noise ratio in epifluorescence imaging
187 experiments. This is especially problematic in bulk dye-loading procedures as Ca^{2+}- or
188 voltage sensitive dyes accumulate differently in different cell-types (i.e. neurons and glial
189 cells), leading to a large variability in fluorescence intensity. To address this issue, we
190 implemented ROI and perisomatic background correction algorithms into NOSA (**Fig. 4B, C**).
191 To demonstrate their utility, we analyzed epileptiform activity in hippocampal slices (Kovacs
192 et al., 2001) (**Fig. 4B**). Here, strong and synchronized increases in fluorescence in CA3
193 neurons lead to increased light-scattering, affecting the SNR in glial cells. However, ROI and
194 perisomatic background correction both successfully reduce the effects of scattered light,
195 increasing the SNR in the activity pattern of a glial cell (**Fig. 4C**).

196 **Combined *in vivo* optical and classical electrophysiology**

197 Being able to compare optical measurements alongside ongoing electrical recordings is
198 useful in many ways. To our knowledge, NOSA is the first open-access tool to provide the
199 option for analyzing optical and electrical traces in parallel. For example, we performed
200 simultaneous patch-clamp and optical recordings *in vivo* from R5 ring neurons and uploaded
201 optical and electrical traces (abf files/ axon binary file format) into NOSA (**Suppl. Fig. 3**). As
202 these traces may be recorded with different systems, temporal delays between the systems
203 could falsify a direct comparison. We implemented an offset function into NOSA, which
204 allows shifting one trace in relation to the other (**Suppl. Fig. 3**). Comparing optical and
205 electrical traces demonstrates that ArcLight faithfully represents changes in membrane
206 potential (**Fig. 5A-C**) and that a change in relative fluorescence of 2% approximates a
207 change of 23 mV in membrane potential (**Fig. 5A-C**). However, the relation between changes
208 in fluorescence and absolute membrane potential will highly depend on the expression
209 strength and must therefore be determined for each cell type. To simplify a direct comparison
210 NOSA can adjust the sampling rate via interpolation of data points. In this example we
211 reduced the sampling rate of the electrical trace from 10 kHz to 2 kHz smoothing out the
212 spikes on top of the bursts which in this case are not represented in the optical trace (**Fig.
213 5A**).

214 Another important application for simultaneous patch clamp and voltage imaging is to
215 investigate single-cell contributions to population dynamics reflected in compound recordings
216 of neural activity. Here, we use NOSA to compare the activity of a single R5 ring neuron with
217 the dorsal bulb, which is comprised of the dendrites of 10-12 R5 neurons (**Fig. 5D**). Power
218 spectrum analysis shows that the peak frequency of the recorded R5 neuron is also
219 represented in the dendritic compound signal (**Fig. 5E**). However, the power spectrum of the

220 compound signal is much more complex due to the fact that the electrical patterns of several
221 R5 neurons contribute to the compound signal. Correlation analysis suggests that some
222 depolarized states of the single R5 neuron overlap with depolarized states in the compound
223 signal (**Fig. 5F, compare Fig. 5D**).

224 **Cross correlation for analyzing event-based temporal relations**

225 When imaging electrical activity in larger brain areas or even in whole brains NOSA can
226 easily analyze the temporal relations of specific events occurring between different neuronal
227 populations. To demonstrate this, we analyzed *in vivo* whole brain voltage imaging
228 recordings in *Drosophila* (Aimon et al., 2019)(**Fig. 6A**). Stimulation with UV light induced
229 electrical activity in the optic lobes while olfactory stimulation induced activity around the area
230 of the lateral horns and peduncles of the mushroom bodies (**Fig. 6B**), which are both higher
231 olfactory integration centers of the *Drosophila* brain (Heisenberg, 2003; Frechter et al.,
232 2019). Interestingly, the central complex, which processes various sensory modalities (Green
233 et al., 2017; Sun et al., 2017) and is important for basic locomotion (Strauss and Heisenberg,
234 1993; Strauss, 2002), shows spontaneous electrical activity. However, it is not clear whether
235 some of the spontaneous activity originates from the visual or olfactory stimulation (**Fig. 6B**).
236 Rather than detecting actual spikes, NOSAs' spike detection can be used to determine the
237 temporal relation between detected events. Events can be detected using a linear or
238 dynamic threshold (**Fig. 1F**). Moreover, the threshold can be set either manually or based on
239 the standard deviation of the whole recording. The detected events are used to generate a
240 time-dependent event marker (**Fig. 6C, compare Suppl. Fig. 4**). The spike cross correlation
241 function identifies the temporal relation between detected events, demonstrating that
242 olfactory responses in the mushroom bodies and lateral horns are temporally aligned (**Fig.
243 6D**). Moreover, the set event markers and cross correlation analysis reveals that olfactory
244 stimulation generates transient activity in the central complex, while visual stimulation does
245 not lead to a detectable response (**Fig. 6D**).

246 To analyze population dynamics in a mammalian brain we used a previously published
247 recording in which one hemisphere of the olfactory bulb expresses ArcLight while the other
248 expresses GCaMP6f (Storace et al., 2015) (**Fig. 6E**). The dorsal bulb exhibits a distinct
249 temporal organization whereby glomeruli in the caudal bulb tend to be more coupled to
250 respiration than glomeruli in the rostral olfactory bulb (Spors et al., 2006; Wachowiak et al.,
251 2013). To demonstrate how quickly temporal relations can be established with NOSA we
252 used the maxima of the olfactory responses in rostral and caudal glomeruli (**Fig. 6F**) to
253 generate an event-based cross correlogram (**Fig. 6G**). This shows that electrical activity
254 requires about 84 ms to travel from the caudal side of the olfactory bulb to the rostral side
255 (**Fig. 6G**). In comparison, intracellular Ca^{2+} requires about 188 ms. Moreover, at the caudal

256 glomeruli the delay between maxima of electrical activity and intracellular Ca^{2+} is 100 ms
257 (**Fig. 6G**). In contrast to this event-based cross correlation the amplitude cross correlation
258 (**Fig. 6H**) considers the whole recording and is thus influenced by the rhythmic changes in
259 voltage which are a result of the mice's breathing pattern (Storace et al., 2015).

260

Discussion

Here, we report a novel open-source tool box, designed specifically for the analysis and interpretation of multicellular optical electrophysiology. While there is sophisticated software for processing imaging recordings (Romano et al., 2017), NOSA is entirely open access and, to our knowledge, the first analysis software that accounts for challenges specific to optical electrophysiology. In this manuscript we discuss these challenges and provide hands-on solutions to extract and analyze electrical patterns from recordings with low signal-to-noise ratio (SNR).

We demonstrate how high recording speeds necessary to resolve single action potentials drastically reduce the SNR (**Fig. 2, 3**). We therefore implemented baseline fitting and filtering algorithms, which can efficiently extract single action potentials and bursts from optical recordings (**Fig. 1-3**). During voltage imaging, the issue of a low SNR is aggravated by light scattering and movement artefacts for which we implemented background subtraction and movement correction algorithms (**Fig. 4**). We combine these basic but essential features for processing imaging data with sophisticated analysis tools for identifying electrical characteristics (**Fig. 3**) and functional interactions (**Fig. 2 and 6**). NOSA can also be used to investigate the temporal relation of sensory-evoked population dynamics in whole brain recordings in *Drosophila* (**Fig. 6A-D**) and in the olfactory bulb in mice (**Fig. 6E-H**). We here show that NOSA can be used to quickly identify temporal relations between the activity patterns of single cells and neuronal populations, which is crucial for investigating under which conditions neural networks interact with each other.

The properties and limitations of GEVIs affect the optical representation of neuronal activity. For example, the improved kinetics of the red-shifted GEVI Varnam increases the likelihood of resolving single spikes while ArcLight generally yields higher SNR (**Fig. 2**). NOSA can be used to quickly determine the properties of GEVIs. Using NOSA we verify that the GEVI Ace2N has faster kinetics than ArcLight (Gong et al., 2015), especially with respect to the repolarization phase of an action potential (**Fig. 3B**). However, the temporal representation of bursts is similar in both GEVIs (**Fig. 3G**). In fact, during bursts ArcLight yields higher relative changes in fluorescence (**Fig. 3G**). With specific knowledge about the properties and limitations, the adequate GEVI can be chosen for a specific experiment. A comprehensive characterization of the properties of different GEVIs are reported elsewhere (Bando et al., 2019).

NOSA's event detection can be used to extract neuron-specific firing characteristics (**Fig. 3**), enabling the fast identification of specific types of neurons within a population of seemingly homogeneous neurons. This knowledge could then be used to electrically stimulate neurons with specific attributes and analyze their connectivity to other neurons (Antic et al., 2016).

Such sophisticated experiments would benefit from another feature, which is provided by NOSA: the simultaneous analysis of optical and electrical data (**Fig. 5**). Moreover, we show how this feature can be used to analyze single-cell contributions to population dynamics (**Fig. 5D**). This is especially important when trying to understand how a multitude of neurons orchestrate their electrical activities to generate population dynamics, e.g. during sleep (Buzsaki and Draguhn, 2004).

GEVIs are currently improving at a rapid pace, developing towards stronger fluorescence and improved kinetics. However, currently the diverse properties of GEVIs and a missing analytical pipeline represent motivational bottlenecks preventing experimental implementation and widespread use of GEVIs. With NOSA we provide an analytical toolbox that will greatly facilitate the use of GEVIs in studying multicellular electrical patterns, inexorably improving our understanding of functional interactions within neural networks.

Figures

Figure 1. NOSA Interface

A, The file manager shows imported files and contains options for movement correction, temporal cropping, offset correction and interpolation of the recording speed.

B, ROI manager showing added ROIs, which can be renamed and deleted. ROI masks can be generated by copying ROIs into other files.

C, Video panel showing currently selected frame and added ROIs. The recording can be adjusted for brightness and contrast.

D, Average fluorescence intensity of selected ROIs with baseline fitting curve and slide for selecting specific frames of the recording.

E, Processed data showing relative changes in fluorescence over time. Calculation of the relative change in fluorescence is based on recording speed, background subtraction, baseline correction and smoothing.

F, Panel for semi-automatic detection of spikes and bursts. Detected events are indicated with orange arrows and white lines/squares indicating spikes/bursts.

G, Power spectrum analysis based on processed data. If the event shape feature is selected this panel also shows the average shape of detected events.

H, Panel showing spike cross correlation calculated based on detected spikes and amplitude cross correlation calculated based on relative changes in fluorescence.

330 **I,** Control panel for adjusting the settings of each feature.

331

Figure 2

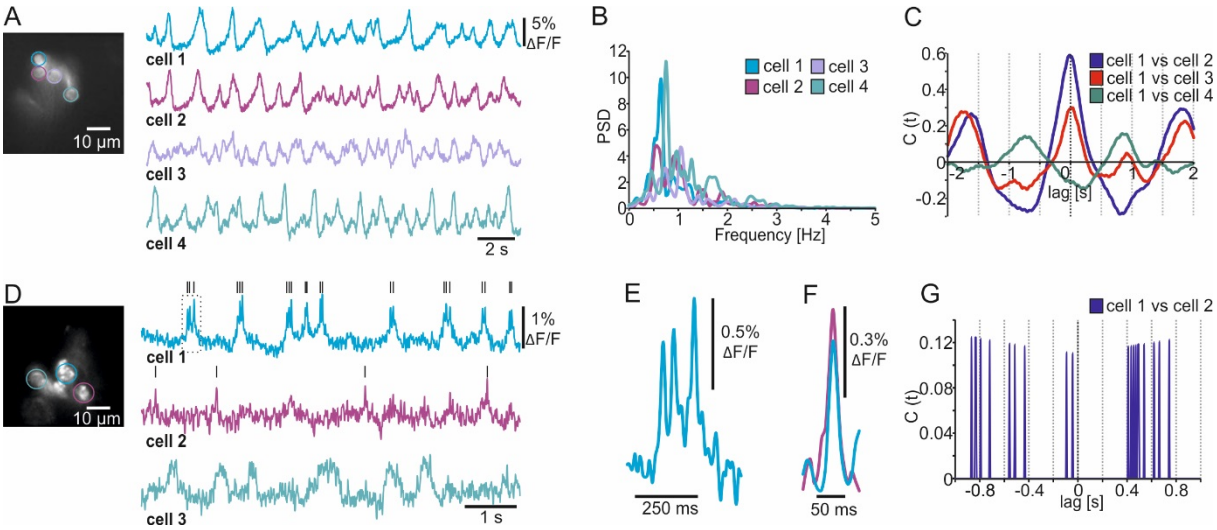

Figure 2. Analyzing multicellular electrical activity from optical recordings

A, Wide-field image and single-cell membrane potential oscillations of *Drosophila* R5 ring neurons expressing the GEVI ArcLight.

B, Power spectrum analysis of R5 electrical activity shown in A.

C, Amplitude cross correlation indicating the temporal relation of R5 electrical patterns shown in A.

D, Wide-field image and single-cell electrical activity of fan-shaped body neurons expressing the GEVI Varnam. Lines indicate detected spikes using a linear threshold approach.

E, Burst (see dashed square in D) showing that Varnam resolves single spikes during bursting.

F, The event shape feature shows the average kinetics of the action potentials detected in cell 1 and 2 (see black lines in D).

G, Spike cross correlation indicating no temporal relations between spikes detected in D.

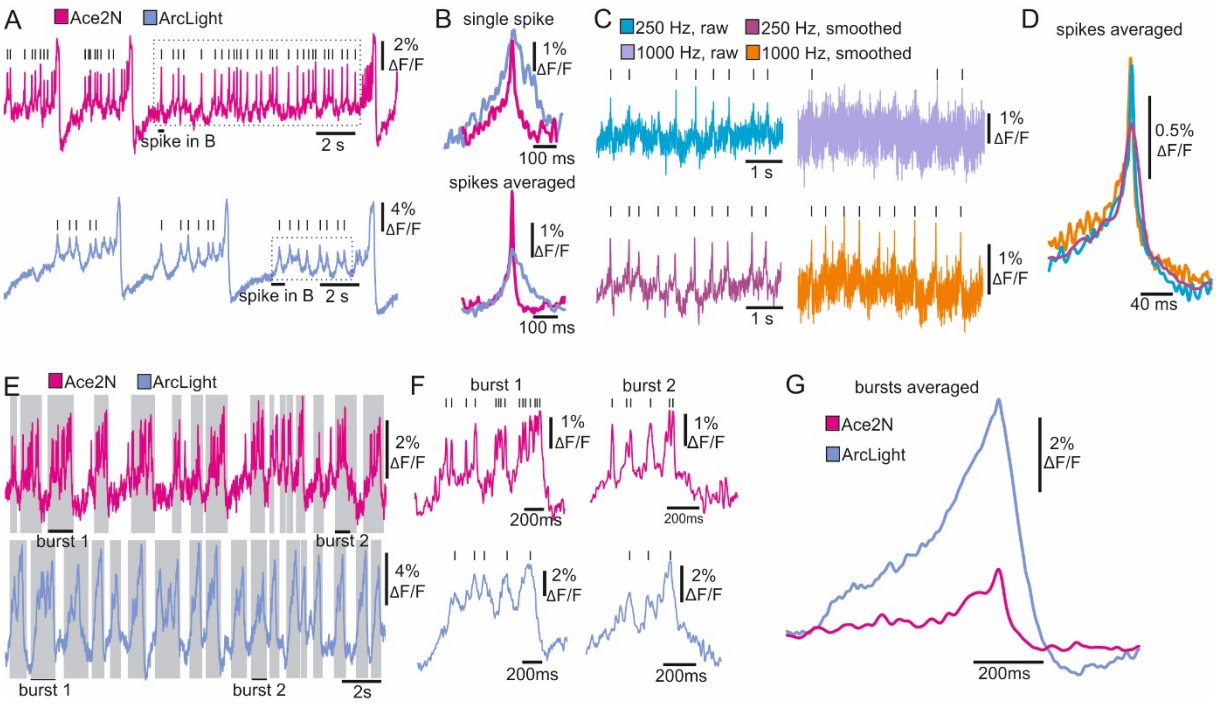

Figure 3. Spike and burst detection revealing kinetic properties of GEVIs and neuron-specific firing characteristics

A, Optical recordings of spiking R5 neurons expressing the GEVIs Ace2N and ArcLight. Lines indicate detected spikes using a linear threshold approach.

B, Single and averaged spikes selected from recordings in A (dashed square indicates spikes selected for event shape). The event shape feature indicates improved kinetics of Ace2N.

C, Optical recordings of a spiking R5 neuron (Ace2N) performed at different recording speeds. Lines indicate identified spikes.

D, The event shape feature shows the average kinetics of spikes detected in C.

E, F, Optical recordings of bursting R5 neurons expressing the GEVIs Ace2N and ArcLight. Grey shaded areas and lines indicate detected bursts and spikes using the dynamic threshold approach.

G, The event shape feature generates the averaged kinetics of detected bursts indicating GEVI-specific differences in the optical representation of bursts.

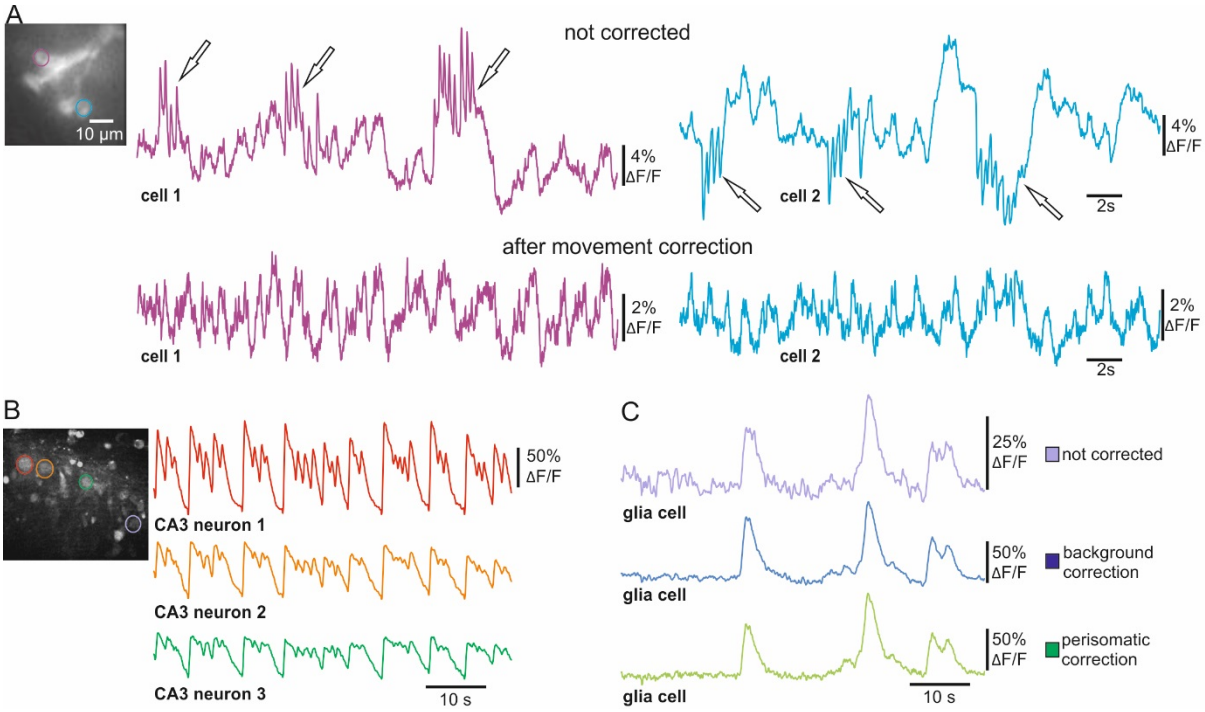

Figure 4. Movement and background correction for voltage and Ca^{2+} imaging

A, *In vivo* voltage imaging (ArcLight) of single R5 neurons before and after performing the symmetric diffeomorphic movement correction.

B, Ca^{2+} imaging from hippocampal slices shows synchronous activity of CA3 neurons after inducing epileptiform activity.

C, Activity of glia cell indicated in wide-field image in B before and after ROI background correction and perisomatic background correction.

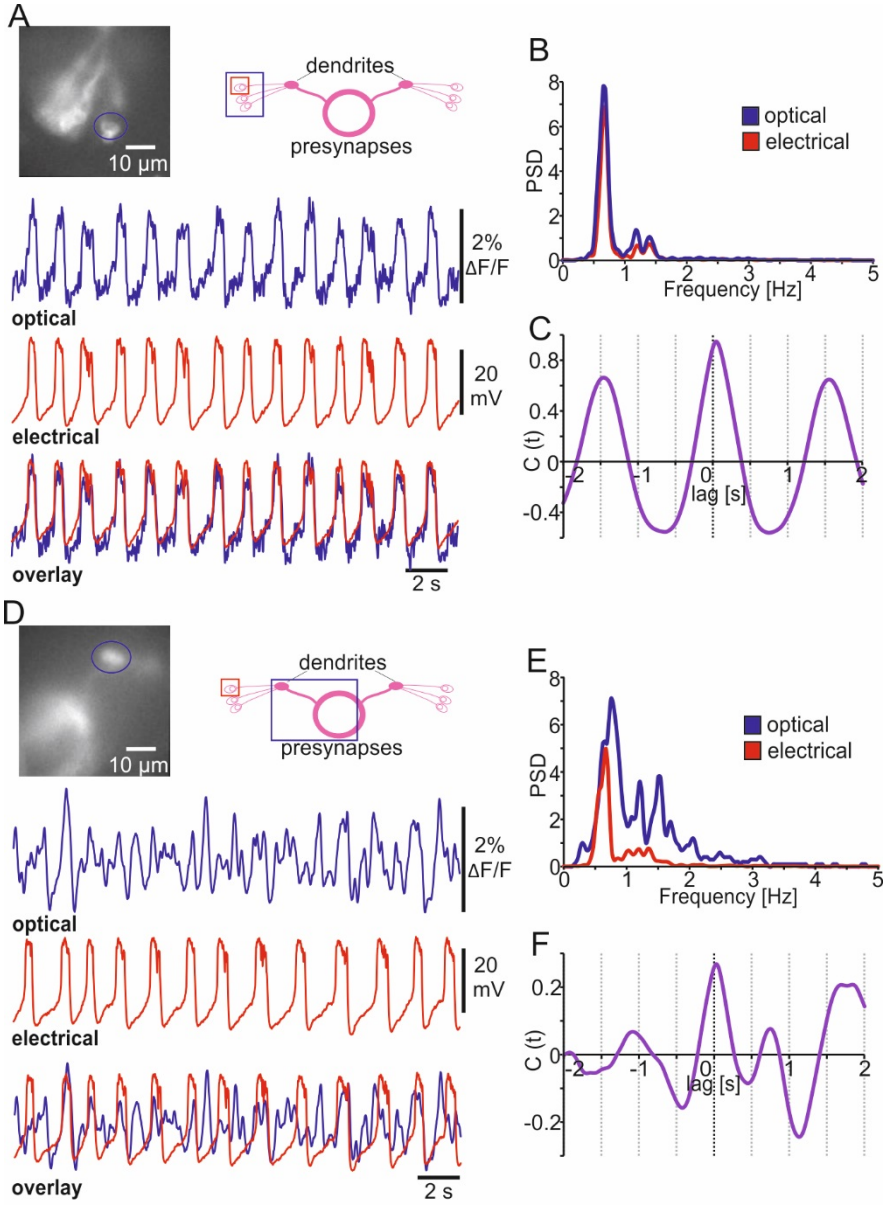

Figure 5. Simultaneous optical and classical electrophysiology

A, Simultaneously recorded *in vivo* optical (ArcLight) and electrical trace (interpolated at 2 kHz) from R5 neuron indicated in the wide-field imaging.

B, Power spectrum analysis of membrane potential oscillations of R5 neuron shown in A.

C, Cross correlograms indicating oscillatory character and temporal overlap of optical and electrical traces shown in A.

D, Simultaneously recorded *in vivo* single-cell patch clamp (interpolated at 2 kHz) and optical compound activity of R5 dendritic area indicated in the wide-field imaging.

E, Power spectrum analysis showing more complex rhythms in the optical compound activity.

384 **F,** Amplitude cross correlation indicating partial temporal overlap between single-cell and
385 compound activity.

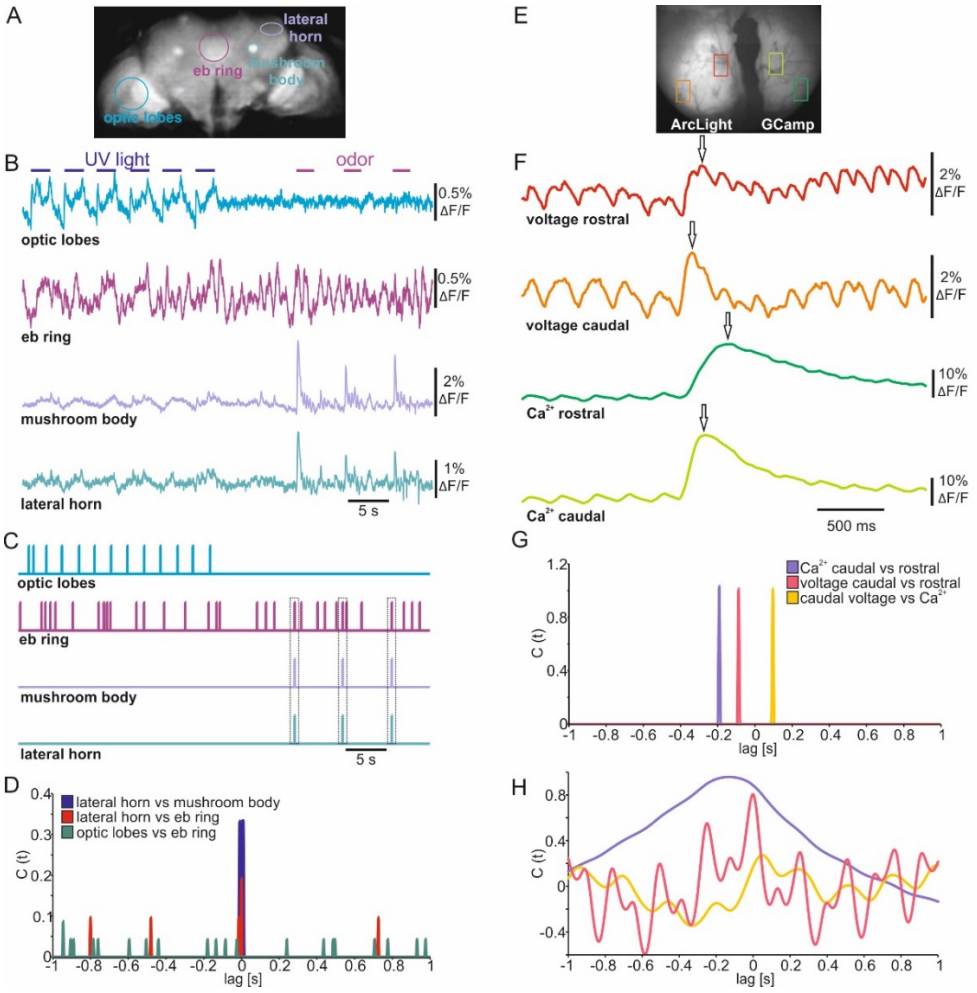

Figure 6. Event cross correlation identifies temporal relations in sensory evoked population dynamics

A, Wide-field image of a mid-section during whole brain voltage imaging (ArcLight) in *Drosophila*.

B, Electrical population activity of different neuropils during optical and olfactory stimulation.

C, Spike detection indicating detected events of electrical activity shown in B.

D, Spike cross correlation indicating temporal shifts between events shown in C. Dashed squares indicate coincidence between olfactory evoked activity and specific events detected in the central complex.

E, Wide-field image of the olfactory bulb injected with ArcLight and GCamp6f in either hemisphere.

F, Olfactory evoked population activity of selected caudal and rostral glomeruli. Arrows indicate detected maxima.

G, Spike cross correlation indicating temporal shifts between maxima indicated in F.

H, Amplitude cross correlation indicating oscillatory character and temporal relations of population dynamics shown in F.

Supplementary Figures

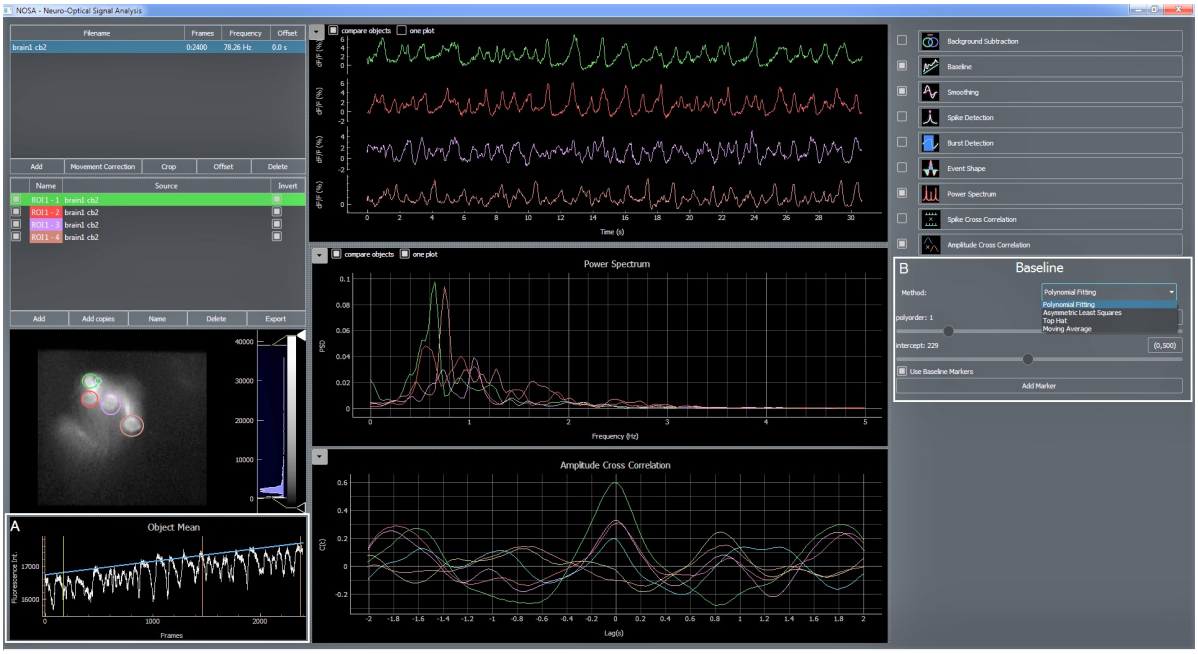

Supplementary figure 1: NOSA baseline correction. Related to Figure 2.

A, Polynomial fitting (blue curve) is used to compensate for baseline drifts and calculate the relative change in fluorescence. Additional baseline markers (orange) can be used to guide the fitting curve.

B, NOSA provides four different algorithms for baseline fitting. For each algorithm, the baseline can be adjusted by changing the shape (polyorder) and position (intercept) of the fitting curve.

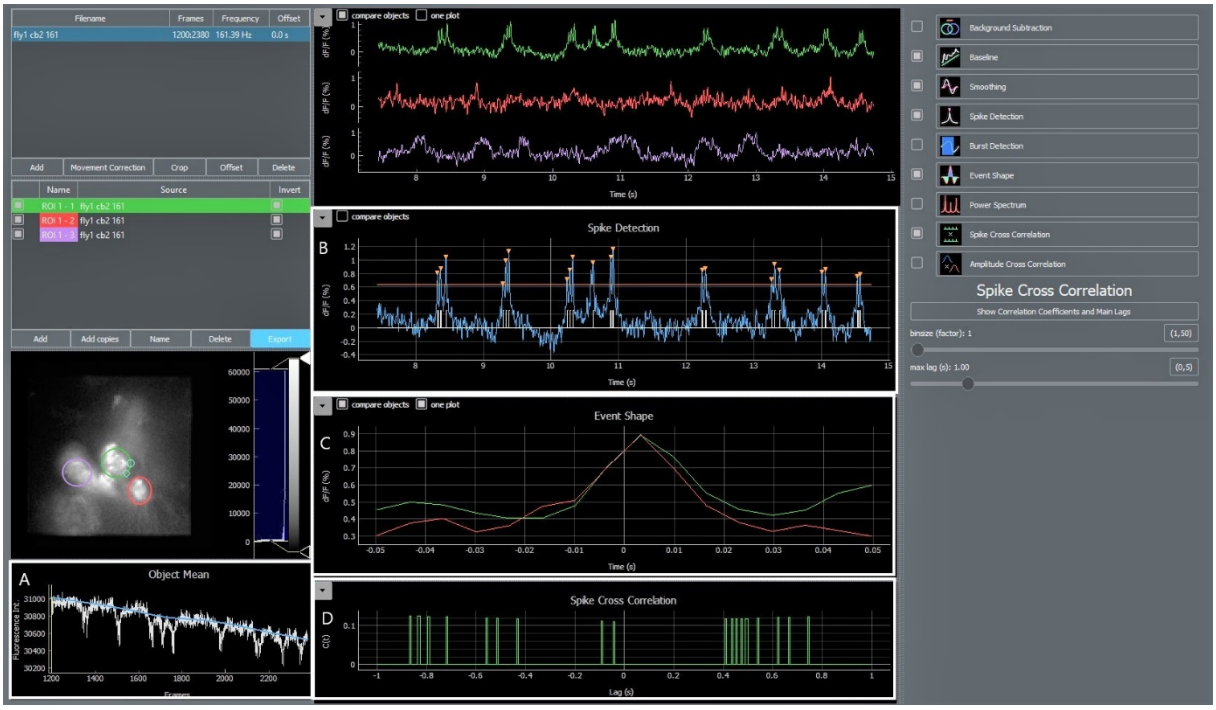

Supplementary figure 2: NOSA spike detection and cross correlation. Related to Figure 2.

A, Shift in baseline fluorescence is corrected via the asymmetric least square algorithm (blue fitting curve).

B, Spike detection using a linear threshold approach. Orange arrows indicate detected spikes.

C, Event shape can be used to generate the average shape of spikes detected in B.

D, NOSA spike cross correlation can be used to analyze the temporal relation between spikes detected in cell 1 (green) and cell 2 (red).

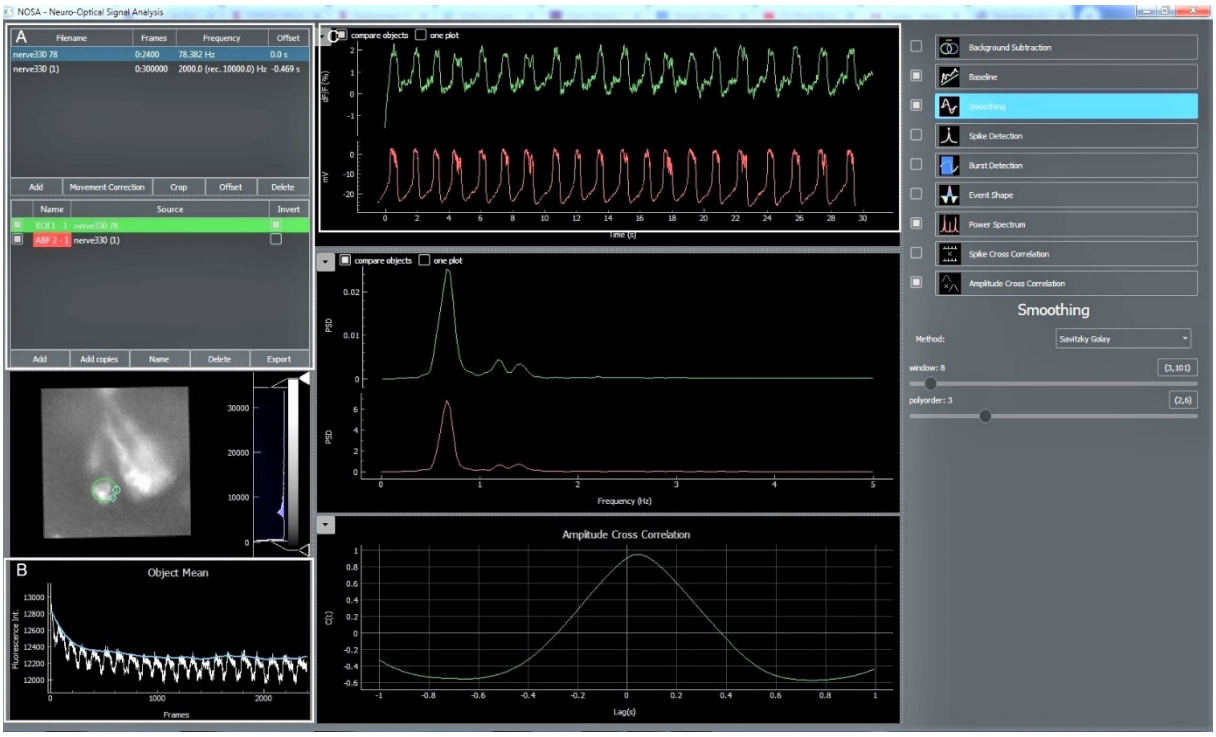

Supplementary figure 3: Simultaneous analysis of optical and electrical recordings. Related to Figure 5.

A, Optical (tiff files) and electrical (abf files) recordings can both be imported into NOSA. Sampling rates and recording speeds can be adjusted via various interpolation algorithms. The sampling rate of the electrical recording (10 kHz) was adjusted to 2 kHz. Delays between the electrical and optical systems can be corrected by an offset function (see C).

B, Optical recording was corrected for bleaching via the asymmetric least square algorithm.

C, The offset function in NOSA (see A) can adjust for temporal delays between the electrical and optical recordings. In this case, the precise delay was 469 ms.

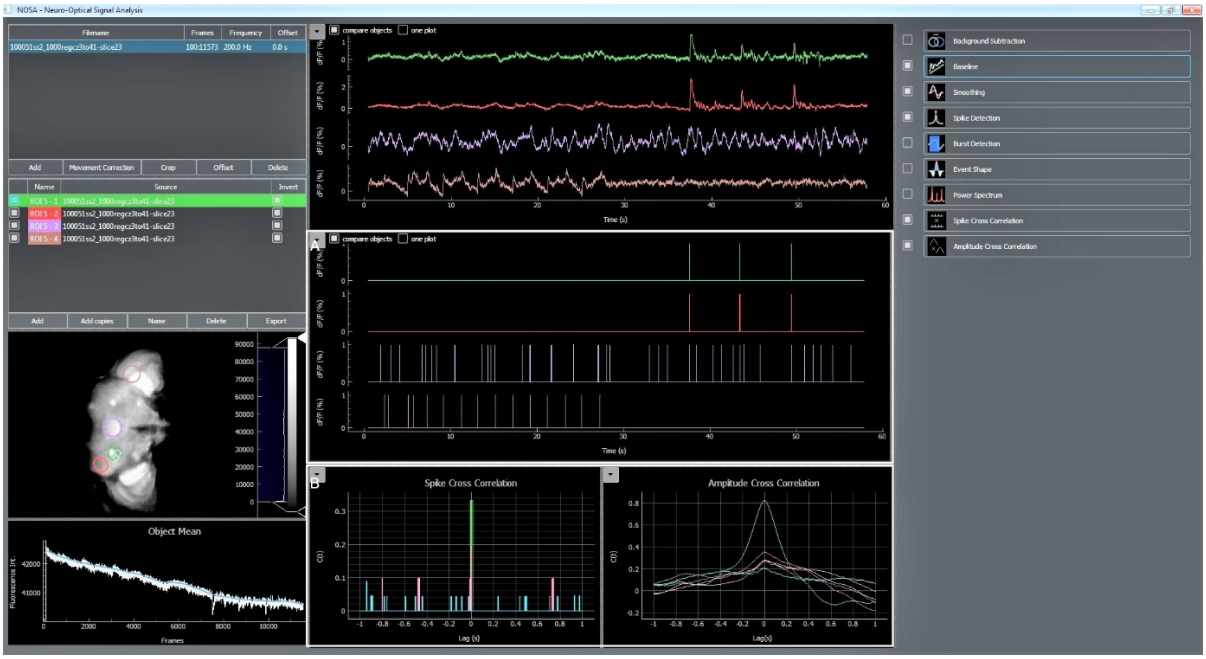

Supplementary figure 4: Combining event detection and cross correlation to identify temporal relations in population dynamics. Related to Figure 6.

A, Spike detection can be used to detect specific events, generating a time-dependent event marker.

B, Spike cross correlation calculates the temporal relation between detected events shown in A. In comparison, the amplitude cross correlation calculates temporal relations based on the relative change in fluorescence.

Methods

NOSA software

NOSA was written in Python 3.7.1 (see https://docs.python.org/3/license.html for license information). Besides default packages and built in functions, NOSA uses a variety of additional packages (**Table 1**). More detailed information on the graphical user interface, the function of specific features, performance aspects and workflow examples are provided in an additional file accompanying the software file. For more information please send an email to the lead contact.

Table 1: Packages used for NOSA

Name	Version	License type	Copyright Notice	Website
NumPy	1.16.2	BSD	Copyright © 2005-2018, NumPy Developers. All rights reserved.	https://www.numpy.org
SciPy	1.2.1	BSD	Copyright © 2001, 2002 Enthought, Inc. All rights reserved. Copyright © 2003-2013 SciPy Developers.All rights reserved.	https://www.scipy.org
PyQt5	5.11.3	GPL v3	Copyright © 2018 Riverbank Computing Limited	https://www.riverbankcomputing.com/software/pyqt/
PyQtGraph	0.10.0	MIT	Copyright (c) 2012 University of North Carolina at Chapel Hill Luke Campagnola ('luke.campagnola@%s.com' % 'gmail')	http://www.pyqtgraph.org
Matplotlib	3.0.3	PSF-based	© Copyright 2002 - 2012 John Hunter, Darren Dale, Eric Firing, Michael Droettboom and the Matplotlib development team; 2012 - 2018 The Matplotlib development team	http://matplotlib.org
pyStackReg	0.2.1	custom	C++ Port of the TurboReg ImageJ Plugin. Original code by	https://bitbucket.org/glichtner/pystackreg

Name	Version	License type	Copyright Notice	Website
			Philippe Thevenaz (Thevenaz et al., 1998). Porting by Gregor Lichtner	
DIPY(Garyfallidis et al., 2014)	0.15.0	revised BSD-2-Clause	Copyright (c) 2008-2019, dipy developers. All rights reserved.	http://dipy.org
QDarkStyle	2.5.4	MIT	Copyright (c) 2013-2018 Colin Duquesnoy.	https://github.com/ColinDuquesnoy/QDarkStyleSheet
neo	0.7.1	BSD-3-Clause	Copyright (c) 2010-2018, Neo authors and contributors.	http://neuralensemble.org/neo
quantities	0.12.3	BSD	Copyright (c) 2012, Darren Dale dsdale24@gmail.com All rights reserved.	http://python-quantities.readthedocs.io/
XlsxWriter	1.1.5	BSD	Copyright (c) 2013, John McNamara jmcnamara@cpan.org All rights reserved.	https://github.com/jmcnamara/XlsxWriter
tifffile	2019.3.8	BSD	Copyright (c) 1994-2019, Christoph Gohlke. All rights reserved.	https://www.lfd.uci.edu/~gohlke/
PyInstaller	3.4	GPL-based	Copyright (c) 2010-2019, PyInstaller Development Team Copyright (c) 2005-2009, Giovanni Bajo Based on previous work under copyright (c) 2002 McMillan Enterprises, Inc.	http://www.pyinstaller.org/
Markdown	1.0.1	BSD-style	Copyright © 2004, John Gruber http://daringfireball.net/ All rights reserved.	https://daringfireball.net/projects/markdown/
markdown-styles	3.1.10	BSD-3-Clause	none provided -- created by GitHub user mixu (Mikito Takada)	https://github.com/mixu/markdown-styles

455 **Optical and classical electrophysiology of R5 neurons in Drosophila melanogaster**

456 Flies (*Drosophila melanogaster*) were reared on standard cornmeal food at 25 °C and 60%
457 humidity under a 12 h light/dark regime. All flies were obtained from the Bloomington Stock
458 resource center (BDRC). Experiments were performed with 3-10 d old female flies at ZT 8-12
459 (Zeitgeber time; during a 12/12 h light/dark cycle the onset of light is at ZT 0 h and the offset
460 of light is at ZT 12 h). Whole-brain explant dissections and fly *in vivo* preparation were
461 performed as previously described (Cao et al., 2013; Owald et al., 2015). During ex vivo
462 experiments (**Fig. 2, 3**) external solution consisted of (in mM): 90 NaCl, 3 KCl, 1.5 $CaCl_2$, 5
463 $MgCl_2$, 1 NaH_2PO_4, 10 glucose, 10 sucrose, 8 trehalose, 5 TES and 26 $NaHCO_3$. During ex
464 vivo experiments (**Fig. 4, 5**) external solution consisted of (in mM): 70 NaCl, 3 KCl, 1.5
465 $CaCl_2$, 20 $MgCl_2$, 1 NaH_2PO_4, 10 glucose, 10 sucrose, 8 trehalose, 5 TES and 26 $NaHCO_3$.

466 Imaging was performed on an Olympus BX51WI microscope using a Plan Apochromat 40×,
467 numerical aperture 0.8, water-immersion objective (Olympus, Japan). ArcLight was excited at
468 470 nm using a Lumencor Spectra X-Light engine LED system. LED power was adjusted for
469 each recording individually to make sure that fluorescent images were not saturated. The
470 objective C-mount image was projected onto an Andor iXon-888 camera controlled by Andor
471 Solis software. Imaging was performed at frame rates of 80 Hz (**Fig. 2A-C, 4 and 5**), 160 Hz
472 (**Fig. 2D-G**) 250 Hz and 1000 Hz (**Fig. 3**).

473 *In vivo* (**Fig. 5**) whole-cell patch-clamp recordings from R5 neurons were performed at ZT 8-
474 12 as reported elsewhere (Wilson and Laurent, 2005; Murthy and Turner, 2013; Donlea et
475 al., 2018). Neurons were recorded for up to 5 min. Identification of R5 neurons was based on
476 ArcLight expression. External saline was used as described above. Patch pipettes (7-10 MΩ)
477 were filled with internal saline containing (mM): 135 K-aspartate, 10 HEPES, 1 EGTA, 1 KCl,
478 4 MgATP, 0.5 Na3GTP. Internal solution was adjusted to a pH of 7.2, with an osmolarity of
479 265 mmol/kg.

480 **Ca^{2+} imaging of hippocampal slices**

481 Animal care and handling was in accordance with the Helsinki declaration and institutional
482 guidelines. Protocols for organ removal and culturing were approved by the State Office of
483 Health and Social Affairs Berlin, under the license number T0123/11. Organotypic
484 hippocampal slice cultures were prepared as described previously (Kann et al., 2011; Prager
485 et al., 2019). In short, hippocampal slices (400 µm) were obtained from Wistar rat pups at
486 postnatal day 6-7. Slices were positioned on cell culture membrane inserts (Millicell-CM,
487 Millipore) and maintained for 6 days in culture medium (50% MEM, 25% HBSS, 25% Horse
488 Serum and 1 mM L-glutamine, pH set to 7.3) at 5% CO_2. At day 7, slice cultures were bulk
489 stained with OGB-1-AM BAPTA (5µM in DMSO, 0.01% Pluronic F-127, 0.005% Cremaphor)

490 by submerging them for 50 min at room temperature in carbogen bubbled serum free
491 medium.

492 Fluorescence recordings were obtained with a spinning disk confocal microscope (Andor
493 Revolution, BFIOptilas GmbH, Gröbenzell, Germany), equipped with an EMCCD camera
494 (Andor iXonEM+, 60x objective N.A.1, 2 x binning, 20 Hz recording speed, laser intensity
495 150-200 µW at the focal level). Slice cultures were superfused with carbogen (95% O_2, 5%
496 CO_2) saturated artificial cerebrospinal fluid containing (in mM): 129 NaCl, 3 KCl, 1.25
497 NaH_2PO_4, 1.8 $MgSO_4$, 1.6 $CaCl_2$, 26 $NaHCO_3$ and 10 glucose (pH 7.4, t=30°C). For induction
498 of synchronized epileptiform activity, Mg^{2+} was omitted and KCl was elevated to 5 mM
499 (Prager et al., 2019).

500 **Whole brain voltage imaging in Drosophila**

501 Whole brain recordings were performed using light field microscopy as described in detail
502 elsewhere (Aimon et al., 2019). In short, a modified upright Olympus BX51W with a 20x NA
503 1.0 XLUMPlanFL (Olympus) was used. An adequate microlens array (RPC Photonics)
504 positioned at the image plane and two relay lenses (50 mm f/1.4 NIKKOR-S Auto from
505 Nikon) projected the image onto the sensor of a scientific CMOS camera (Hamamatsu
506 ORCA-Flash 4.0). A 490 nm LED (pE100 CoolLED) at approximately 10% of its full power
507 was used for excitation. As filter set we used a 482/25 bandpass filter, a 495-nm dichroic
508 beam splitter, and a 520/35 bandpass emission filter (BrightLine, Semrock). The recording
509 was performed at a frame rate of 200 Hz. The whole brain volume was reconstruction from
510 the light field image as described in (Aimon et al., 2019)

511 **Voltage and calcium imaging in the olfactory bulb**

512 Olfactory bulb recordings in mice were performed as described in detail elsewhere (Storace
513 et al., 2015). In short, C57BL/6 mice (JAX, Bar Harbor, MA) were injected into the olfactory
514 bulbs with AAV1 expressing either ArcLight- or GCaMP6f. Mice were anesthetized
515 (ketamine/xylazine) and the bone above both olfactory bulbs was either thinned or removed.
516 The exposure was covered with agarose and sealed with a glass coverslip. The dorsal
517 surface of both hemispheres was illuminated with 485 ± 25 nm light using epifluoresence
518 illumination on a Leitz Ortholux II microscope with a tungsten halogen lamp or a 150 W
519 Xenon arc lamp (Opti Quip) and a 515 nm long-pass dichroic mirror. Fluorescence emission
520 was recorded with a NeuroCCD-SM256 camera with 2 × 2 binning at 125 Hz using NeuroPlex
521 software (RedShirtImaging, Decatur, GA). All surgical procedures were approved by the Yale
522 IACUC.

523

References

Adhikari A, Sigurdsson T, Topiwala MA, Gordon JA (2010) Cross-correlation of instantaneous amplitudes of field potential oscillations: a straightforward method to estimate the directionality and lag between brain areas. J Neurosci Methods 191:191-200.

Aimon S, Katsuki T, Jia T, Grosenick L, Broxton M, Deisseroth K, Sejnowski TJ, Greenspan RJ (2019) Fast near-whole-brain imaging in adult Drosophila during responses to stimuli and behavior. PLoS Biol 17:e2006732.

Alivisatos AP, Chun M, Church GM, Greenspan RJ, Roukes ML, Yuste R (2012) The brain activity map project and the challenge of functional connectomics. Neuron 74:970-974.

Antic SD, Empson RM, Knopfel T (2016) Voltage imaging to understand connections and functions of neuronal circuits. J Neurophysiol 116:135-152.

Avants BB, Epstein CL, Grossman M, Gee JC (2008) Symmetric diffeomorphic image registration with cross-correlation: evaluating automated labeling of elderly and neurodegenerative brain. Med Image Anal 12:26-41.

Azimi Hashemi N, Bergs ACF, Schuler C, Scheiwe AR, Steuer Costa W, Bach M, Liewald JF, Gottschalk A (2019) Rhodopsin-based voltage imaging tools for use in muscles and neurons of Caenorhabditis elegans. Proc Natl Acad Sci U S A 116:17051-17060.

Bando Y, Sakamoto M, Kim S, Ayzenshtat I, Yuste R (2019) Comparative Evaluation of Genetically Encoded Voltage Indicators. Cell Rep 26:802-813 e804.

Buzsaki G, Draguhn A (2004) Neuronal oscillations in cortical networks. Science 304:1926-1929.

Cao G, Platisa J, Pieribone VA, Raccuglia D, Kunst M, Nitabach MN (2013) Genetically targeted optical electrophysiology in intact neural circuits. Cell 154:904-913.

Donlea JM, Pimentel D, Miesenbock G (2014) Neuronal machinery of sleep homeostasis in Drosophila. Neuron 81:860-872.

Donlea JM, Pimentel D, Talbot CB, Kempf A, Omoto JJ, Hartenstein V, Miesenbock G (2018) Recurrent Circuitry for Balancing Sleep Need and Sleep. Neuron 97:378-389 e374.

Frechter S, Bates AS, Tootoonian S, Dolan MJ, Manton J, Jamasb AR, Kohl J, Bock D, Jefferis G (2019) Functional and anatomical specificity in a higher olfactory centre. Elife 8.

Garyfallidis E, Brett M, Amirbekian B, Rokem A, van der Walt S, Descoteaux M, Nimmo-Smith I, Dipy C (2014) Dipy, a library for the analysis of diffusion MRI data. Front Neuroinform 8:8.

Gong Y, Huang C, Li JZ, Grewe BF, Zhang Y, Eismann S, Schnitzer MJ (2015) High-speed recording of neural spikes in awake mice and flies with a fluorescent voltage sensor. Science 350:1361-1366.

Green J, Adachi A, Shah KK, Hirokawa JD, Magani PS, Maimon G (2017) A neural circuit architecture for angular integration in Drosophila. Nature 546:101-106.

Guo F, Holla M, Diaz MM, Rosbash M (2018) A Circadian Output Circuit Controls Sleep-Wake Arousal in Drosophila. Neuron 100:624-635 e624.

Heisenberg M (2003) Mushroom body memoir: from maps to models. Nat Rev Neurosci 4:266-275.

Hu W, Peng Y, Sun J, Zhang F, Zhang X, Wang L, Li Q, Zhong Y (2018) Fan-Shaped Body Neurons in the Drosophila Brain Regulate Both Innate and Conditioned Nociceptive Avoidance. Cell Rep 24:1573-1584.

Kann O, Huchzermeyer C, Kovacs R, Wirtz S, Schuelke M (2011) Gamma oscillations in the hippocampus require high complex I gene expression and strong functional performance of mitochondria. Brain 134:345-358.

Kannan M, Vasan G, Huang C, Haziza S, Li JZ, Inan H, Schnitzer MJ, Pieribone VA (2018) Fast, in vivo voltage imaging using a red fluorescent indicator. Nat Methods 15:1108-1116.

Kovacs R, Schuchmann S, Gabriel S, Kardos J, Heinemann U (2001) Ca2+ signalling and changes of mitochondrial function during low-Mg2+-induced epileptiform activity in organotypic hippocampal slice cultures. Eur J Neurosci 13:1311-1319.

Kulkarni RU, Miller EW (2017) Voltage Imaging: Pitfalls and Potential. Biochemistry 56:5171-5177.

Lin MZ, Schnitzer MJ (2016) Genetically encoded indicators of neuronal activity. Nat Neurosci 19:1142-1153.
Liu S, Liu Q, Tabuchi M, Wu MN (2016) Sleep Drive Is Encoded by Neural Plastic Changes in a Dedicated Circuit. Cell 165:1347-1360.
Miyazawa H, Okumura K, Hiyoshi K, Maruyama K, Kakinuma H, Amo R, Okamoto H, Yamasu K, Tsuda S (2018) Optical interrogation of neuronal circuitry in zebrafish using genetically encoded voltage indicators. Sci Rep 8:6048.
Murthy M, Turner G (2013) Whole-cell in vivo patch-clamp recordings in the Drosophila brain. Cold Spring Harb Protoc 2013:140-148.
Owald D, Felsenberg J, Talbot CB, Das G, Perisse E, Huetteroth W, Waddell S (2015) Activity of defined mushroom body output neurons underlies learned olfactory behavior in Drosophila. Neuron 86:417-427.
Prager O, Kamintsky L, Hasam-Henderson LA, Schoknecht K, Wuntke V, Papageorgiou I, Swolinsky J, Muoio V, Bar-Klein G, Vazana U, Heinemann U, Friedman A, Kovacs R (2019) Seizure-induced microvascular injury is associated with impaired neurovascular coupling and blood-brain barrier dysfunction. Epilepsia 60:322-336.
Raccuglia D, Yan McCurdy L, Demir M, Gorur-Shandilya S, Kunst M, Emonet T, Nitabach MN (2016) Presynaptic GABA Receptors Mediate Temporal Contrast Enhancement in Drosophila Olfactory Sensory Neurons and Modulate Odor-Driven Behavioral Kinetics. eNeuro 3.
Raccuglia D, Huang S, Ender A, Heim MM, Laber D, Suarez-Grimalt R, Liotta A, Sigrist SJ, Geiger JRP, Owald D (2019) Network-Specific Synchronization of Electrical Slow-Wave Oscillations Regulates Sleep Drive in Drosophila. Curr Biol 29:3611-3621 e3613.
Romano SA, Perez-Schuster V, Jouary A, Boulanger-Weill J, Candeo A, Pietri T, Sumbre G (2017) An integrated calcium imaging processing toolbox for the analysis of neuronal population dynamics. PLoS Comput Biol 13:e1005526.
Seelig JD, Jayaraman V (2013) Feature detection and orientation tuning in the Drosophila central complex. Nature 503:262-266.
Spors H, Wachowiak M, Cohen LB, Friedrich RW (2006) Temporal dynamics and latency patterns of receptor neuron input to the olfactory bulb. J Neurosci 26:1247-1259.
Storace D, Sepehri Rad M, Kang B, Cohen LB, Hughes T, Baker BJ (2016) Toward Better Genetically Encoded Sensors of Membrane Potential. Trends Neurosci 39:277-289.
Storace DA, Cohen LB (2017) Measuring the olfactory bulb input-output transformation reveals a contribution to the perception of odorant concentration invariance. Nat Commun 8:81.
Storace DA, Braubach OR, Jin L, Cohen LB, Sung U (2015) Monitoring brain activity with protein voltage and calcium sensors. Sci Rep 5:10212.
Strauss R (2002) The central complex and the genetic dissection of locomotor behaviour. Current Opinion in Neurobiology 12:633-638.
Strauss R, Heisenberg M (1993) A higher control center of locomotor behavior in the Drosophila brain. J Neurosci 13:1852-1861.
Sun Y, Nern A, Franconville R, Dana H, Schreiter ER, Looger LL, Svoboda K, Kim DS, Hermundstad AM, Jayaraman V (2017) Neural signatures of dynamic stimulus selection in Drosophila. Nat Neurosci 20:1104-1113.
Thevenaz P, Ruttimann UE, Unser M (1998) A pyramid approach to subpixel registration based on intensity. IEEE Trans Image Process 7:27-41.
Wachowiak M, Economo MN, Diaz-Quesada M, Brunert D, Wesson DW, White JA, Rothermel M (2013) Optical dissection of odor information processing in vivo using GCaMPs expressed in specified cell types of the olfactory bulb. J Neurosci 33:5285-5300.
Wilson RI, Laurent G (2005) Role of GABAergic inhibition in shaping odor-evoked spatiotemporal patterns in the Drosophila antennal lobe. J Neurosci 25:9069-9079.
Yang HH, St-Pierre F (2016) Genetically Encoded Voltage Indicators: Opportunities and Challenges. J Neurosci 36:9977-9989.